

Tuning of photocatalytic activity by creating a tridentate coordination sphere for palladium†

Cite this: *Dalton Trans.*, 2014, **43**, 11676M. G. Pfeffer,^a L. Zedler,^b S. Kupfer,^b M. Paul,^b M. Schwalbe,^c K. Peuntinger,^d D. M. Guldi,^d J. Guthmuller,^e J. Popp,^f S. Gräfe,^f B. Dietzek^f and S. Rau^{*a}

The synthesis and characterisation of an asymmetric potential bridging ligand **bmpmpphz** (**bmpmpphz** = 2,17-bis(4-methoxyphenyl)tetrapyrido[3,2-*a*:2',3'-*c*:3''-*h*:2''',3'''-*j*] phenazine) is presented. This ligand contains a 1,10-phenanthroline (phen) and a 2,9-disubstituted phen sphere and possesses a strong absorbance in the visible. Facile coordination of the phen sphere to a Ru(tbbpy)₂ core leads to **Ru(bmpmpphz)** ([tbbpy]₂Ru(bmpmpphz))(PF₆)₂; tbbpy = 4,4'-di-*tert*-butyl-2,2'-bipyridine). UV-vis, emission, resonance Raman and theoretical investigations show that this complex possesses all properties associated with a **Ru(tpphz)** ([tbbpy]₂Ru(tpphz))(PF₆)₂; tpphz = tetrapyrido[3,2-*a*:2',3'-*c*:3''-*h*:2''',3'''-*j*] phenazine) moiety and that the ligand based absorbances in the vis-part also populate an MLCT like state. The coordination of a Pd-core in the new 2,9-disubstituted phen sphere is possible, leading to a cyclometallation. The tridentate complexation leads to changes in the UV-vis and emission behaviour. Furthermore, the stability of the Pd-coordination is significantly enhanced if compared to the unsubstituted **Ru(tpphz)**. **Ru(bmpmpphz)PdCl** proved to be an active photocatalyst for H₂ evolution, albeit with lower activity than the mother compound **Ru(tpphz)PdCl₂**.

Received 11th April 2014,
Accepted 16th June 2014

DOI: 10.1039/c4dt01034e

www.rsc.org/dalton

Introduction

The photocatalytic splitting of water into molecular hydrogen and oxygen could provide the key to clean and unlimited energy.¹ Over the last decades, different concepts to convert light energy into chemical energy were published. Beside heterogeneous systems, which usually require inorganic² or organic³ semiconductors with an expedient band gap matching the redox potentials for water splitting, also homogeneous catalysts revealed promising properties to produce hydrogen^{4–9} and oxygen^{10–16} from water using sunlight as energy source.

One of the first homogeneous systems for light-driven hydrogen generation consisted of Ru(bpy)₃²⁺ (bpy = 2,2'-bipyridine) as photosensitizer for light absorption, colloidal platinum as hydrogen producing catalyst and Rh(bpy)₃³⁺ as electron relay to store and transfer electrons from the ruthenium chromophore to the platinum catalyst.¹⁷ Relatively recent developments are intramolecular systems, in which the photosensitizer, the electron relay and the catalyst are combined in one single molecule forming a photochemical molecular device (PMD).^{18,19}

Both, intermolecular as well as intramolecular assemblies can serve as highly efficient hydrogen evolving systems. However, in order to perform detailed investigations on the actual reaction mechanism, intramolecular catalysts are directly accessible for mechanistic investigations, as their functionality does not depend on diffusion and collision processes. Thus, by modifying the individual subunits of an intramolecular photocatalyst, *i.e.* either the photocentre, the bridging ligand or the catalytic centre, structure–activity relationships can be established and the photocatalyst's performance, *e.g.* catalytic efficiency can be tuned.^{20–25}

The intensively studied intramolecular photocatalyst [(tbbpy)₂Ru(tpphz)PdCl₂](PF₆)₂ (Fig. 1, **Ru(tpphz)PdCl₂**; tbbpy = 4,4'-di-*tert*-butyl-2,2'-bipyridine, tpphz = tetrapyrido[3,2-*a*:2',3'-*c*:3''-*h*:2''',3'''-*j*]phenazine) is an active hydrogen evolving PDM generating H₂ with a maximum turnover number (TON) of 238.²⁶

^aUniversity of Ulm, Institute of Inorganic Chemistry Materials and Catalysis, Albert-Einstein-Allee 11, 89081 Ulm, Germany. E-mail: sven.rau@uni-ulm.de; Fax: +49 731 5023039; Tel: +49 731 5023900

^bInstitute of Physical Chemistry, Friedrich-Schiller-University Jena, Helmholtzweg 4, 07743 Jena, Germany

^cDepartment of Chemistry, Humboldt-Universität zu Berlin, Metalorganic Chemistry and Photochemistry, Brook-Taylor-Strasse 2, 12489 Berlin, Germany

^dPhysikalische Chemie I, Department of Chemistry and Pharmacy and Interdisciplinary Center for Molecular Materials, Friedrich-Alexander-Universität Erlangen-Nürnberg, Egerlandstr. 3, 91058 Erlangen, Germany

^eFaculty of Applied Physics and Mathematics, Gdansk University of Technology, Narutowicza 11/12, 80233 Gdansk, Poland

^fInstitute of Physical Chemistry and Abbe Center of Photonics, Friedrich-Schiller-University Jena, Helmholtzweg 4, D-07743 Jena, Germany

† Electronic supplementary information (ESI) available. See DOI: 10.1039/c4dt01034e

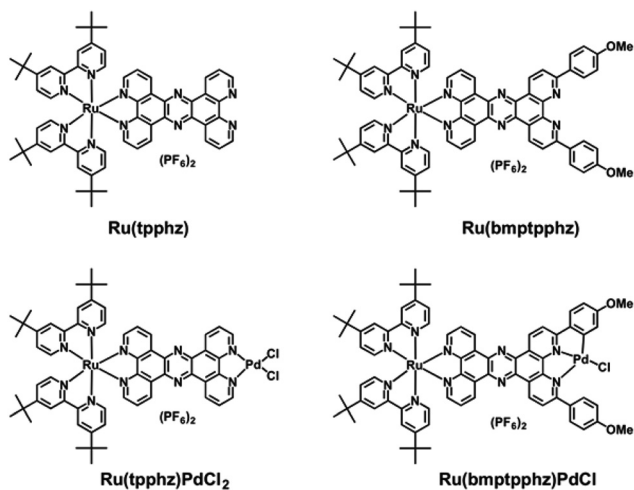


Fig. 1 Top: Mononuclear complexes $[(tbbpy)_2Ru(tpphz)PdCl_2](PF_6)_2$ (**Ru(tpphz)**, left) and $[(tbbpy)_2Ru(bmptpphz)](PF_6)_2$ (**Ru(bmptpphz)**, right). Bottom: dinuclear photocatalysts $[(tbbpy)_2Ru(tpphz)PdCl_2](PF_6)_2$ (**Ru(tpphz)PdCl₂**, left) and $[(tbbpy)_2Ru(bmptpphz)PdCl](PF_6)_2$ (**Ru(bmptpphz)PdCl**, right).

Hereby, the tpphz bridging ligand does not only act as a link of two metal centres and as electron reservoir,^{27,28} but also as tuneable electron relay. For instance, it could be shown that the introduction of bromo substituents at the ruthenium faced 1,10-phenanthroline (phen) part of the tpphz ligand significantly affects the catalytic activity, by means of a decrease of the maximum TON from 238 to 94.²⁹

Typical for PMDs, tuning of the bridging ligand does not change the mechanism and general function of the photocatalyst.¹⁸ Independent from the substitution pattern of the tpphz bridging ligand, the photocatalytic reaction starts with an excitation of the ruthenium photocentre by visible light irradiation (470 nm) to a ¹MLCT (metal to ligand charge transfer) state, which relaxes within less than 1 ps to the corresponding ³MLCT state located on the phen part of tpphz facing the ruthenium centre. This is followed by an electron transfer to the phenazine moiety of the bridging ligand. Upon a simultaneous dissociation of a chloride from the palladium centre, the electron is finally transferred to the catalytic metal centre, which is reduced from Pd(II) to Pd(I).^{30,31} So far, subsequent mechanistic steps taking place until molecular hydrogen is finally abstracted from the catalytic metal centre have remained vague.

Hammarström *et al.* studied a structurally related dinuclear Ru–Pd complex containing a PdCl₂ unit bound to a bipyridine ligand, which is capable of generating hydrogen from a mixture of acetonitrile and triethylamine, the latter functioning as both, electron donor and proton source.³² *Via* gas chromatography (GC), X-ray photoelectron spectroscopy (XPS) and transmission electron spectroscopy (TEM) experiments they could show that the Ru–Pd complex is an active photocatalyst, however the hydrogen evolution goes along with the formation of colloidal Pd(0). Moreover an induction period was observed without any formation of hydrogen, which has

been suggested to be related to the photodecomposition and formation of colloidal catalyst. Thus, it must be assumed that a heterogeneous pathway through palladium colloids might have a contribution to the photocatalytic formation of hydrogen. We have recently shown that also in **Ru(tpphz)PdCl₂** colloid formation takes place during catalytic turnover.³³ By X-ray absorption spectroscopy (XAS), a fast and significant accumulation of Pd(0) colloids as a function of irradiation time was detected. However, from these experiments it is not finally clarified whether Pd(0) colloids function as an essential intermediate for the evolution of molecular hydrogen or are just a catalytically inactive decomposition product.

In general, the formation of colloidal palladium takes place if the stability of the zero valent metal centre in the corresponding ligand sphere is too low. This problem can be addressed by manipulating the corresponding ligand environment, as frequently utilised in organometallic catalysis. Within the context of phen like ligands for organometallic catalysts detailed studies have shown that catalysts based on palladium complexes with 2,9-diaryl substituted phen ligands induce increased selectivity and specificity in the ring opening copolymerisation of alkenes and carbon monoxide compared to unsubstituted phen catalysts.³⁴ We therefore were intrigued by the possibility to stabilise the palladium centre in tpphz based dinuclear complexes by a similar change of substitution pattern.

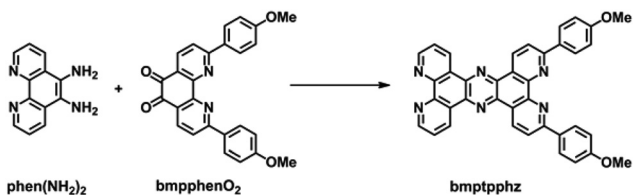
Here, we report on the synthesis, as well as on the characterisation of two novel complexes $[(tbbpy)_2Ru(bmptpphz)](PF_6)_2$ **Ru(bmptpphz)** and $[(tbbpy)_2Ru(bmptpphz)PdCl](PF_6)_2$ **Ru(bmptpphz)PdCl** (Fig. 1). Steady-state absorption-, emission- and resonance Raman spectroscopy as well as cyclic voltammetry, were applied to gain information on the effect of the novel substitution pattern on the photophysical and electrochemical properties of **Ru(bmptpphz)**. Finally, photocatalysis and mercury poisoning experiments with **Ru(bmptpphz)PdCl** were investigated to examine the contribution of Pd(0) colloids to the formation of molecular hydrogen.

Results and discussion

Synthesis and characterization

Since a direct regioselective substitution of tpphz is hard to realize due to its insolubility, the novel 2,17-arylated bridging ligand **bmptpphz** was built up in a stepwise manner (see ESI Scheme S1†).

Therefore, first the 2,9-bis(4-methoxyphenyl)phenanthroline-5,6-dione (**bmpphenO₂**) building block was synthesised, mostly according to a synthetic route that Sauvage *et al.* recently published.³⁵ To obtain the **bmptpphz** ligand, **bmpphenO₂** was reacted with phenanthroline-5,6-diamine (phen(NH₂)₂) (76% yield, Scheme 1). Therefore, to a solution of **bmpphenO₂** in dry methanol, phen(NH₂)₂ was added in portions to avoid a possible self-condensation of phen(NH₂)₂ to tpphz. Finally, the complexation of the obtained ligand **bmptpphz** with $[(tbbpy)_2RuCl_2]$ (tbbpy = 4,4'-di-*tert*-butyl-2,2'-



Scheme 1 Synthesis of **bmptpphz**: methanol, reflux, 8 h (76%).

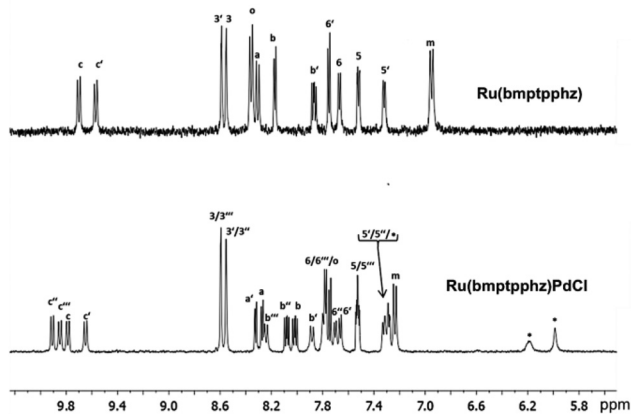


Fig. 2 Aromatic region of the $^1\text{H-NMR}$ spectra in acetonitrile- d_6 of **Ru(bmptpphz)** (top, $c = 5 \times 10^{-4}$ M) and **Ru(bmptpphz)PdCl** (bottom, $c = 8.5 \times 10^{-3}$ M).

bipyridine) was carried out in ethanol–water at reflux to obtain the brownish target molecule **Ru(bmptpphz)** in 78% yield. In comparison, the complexation of the unsubstituted tpphz with $[(\text{tbbpy})_2\text{RuCl}_2]$ has to be performed at 200 °C in refluxing ethylene glycol with a three-fold excess of the ligand to guarantee a sufficient solvation of tpphz and to avoid a complexation of the ruthenium moiety on both coordination sites.³⁰

In the case of the methoxyphenyl-substituted tpphz ligand much milder conditions, *i.e.* a 1 : 1 ratio of the reactants and a lower reaction temperature, are sufficient, since the likelihood of a double complexation is strongly reduced due to steric hindrance of the bulky substituents in *ortho*-position to the nitrogens.

To confirm the structure of the novel ruthenium complex **Ru(bmptpphz)** a series of characterization methods was applied. The set of proton signals in the $^1\text{H-NMR}$ spectrum was in good agreement with the compound's structure and proved its purity (see Fig. 2 and Experimental section). Additionally, recording of a two-dimensional H,H-COSY spectrum allowed for the clear assignment of all signals. Furthermore, $^{13}\text{C-NMR}$ spectroscopy and mass spectrometry provided extra convincing evidence for the structure of **Ru(bmptpphz)** (Scheme 2).

Finally, the mononuclear ruthenium complex **Ru(bmptpphz)** was reacted with $(\text{acn})_2\text{PdCl}_2$ to obtain the dinuclear complex **Ru(bmptpphz)PdCl**. Thereby, a subsequent *ortho* C–H activation by the introduced palladium centre was

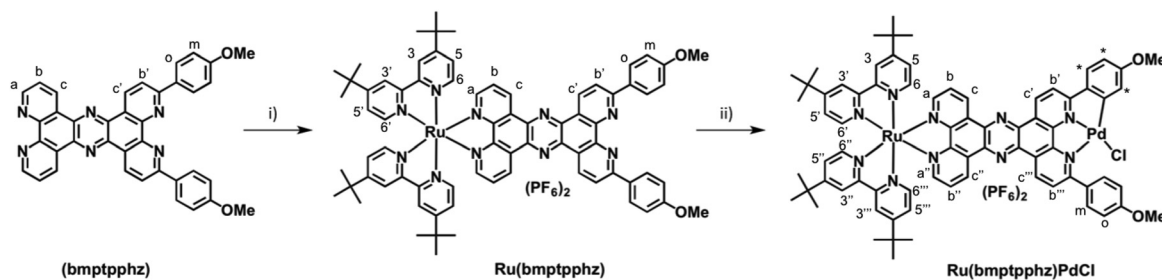
observed, leading to a tridentate NNC-coordination motif. Similar behaviour was observed for Pd-chloro complexes with 6-phenyl-bipyridine.^{36–39} As the cyclometallation leads to a loss of the C_{2v} symmetry, the aromatic proton signals in the ^1NMR spectrum are split into a new set of signals for **Ru(bmptpphz)-PdCl** (Fig. 2).

The $^1\text{H-NMR}$ signals were assigned *via* H,H-COSY NMR spectroscopy. The structure of the dinuclear complex was additionally confirmed *via* ESI mass spectrometry.

Steady state UV-vis and emission spectroscopy

Fig. 3 (dotted line) and Table 1 show the absorption properties of **bmptpphz** in acetonitrile. The novel bridging ligand has two main maxima in the UV region at 305 and 341 nm and also a pronounced absorption feature in the visible region with the maximum at 413 nm ($\epsilon = 32 \times 10^3 \text{ M}^{-1} \text{ cm}^{-1}$), these bands have been assigned based on TDDFT simulations to bright excitations into the states S_9 and S_8 , the S_4 , and the S_1 of intra-ligand charge transfer (ILCT) character (see Fig. S8a, Table S5 and Fig. S9† for more details). This is remarkable, as the unsubstituted tpphz only absorbs at wavelengths below 400 nm.^{40,41} Even the bis(4-butylphenyl)tpphz shows an absorption maximum only at 393 nm. These data suggest that the absorption of visible light is associated with the novel substitution pattern, which is supported by TDDFT calculations on the mononuclear ruthenium complex, described in the following paragraph.

The complexation of **bmptpphz** with $(\text{tbbpy})_2\text{RuCl}_2$ forming **Ru(bmptpphz)** leads to a combination of ligand and ruthenium based absorption properties (Fig. 3, solid line). Thereby, three main absorption bands are detected in the UV region, which can be assigned based on the quantum chemical simulations to first, excitations of the π system of the tbbpy ligands (287 nm). Second, the phen part of the **bmptpphz** ligand causes a shoulder at 312 nm and can be assigned to the excited states S_{29} , S_{30} , S_{32} , and S_{50} . Third, the phenazine moiety at 351 nm associated to S_{20} .^{29,40–42} Further details with respect to the excited states are provided in the ESI (Table S6, Fig. S8b and S10†). In comparison to **Ru(tpphz)** (Fig. 3, dashed line), which shows a typical broad MLCT band at 445 nm ($\epsilon = 20 \times 10^3 \text{ M}^{-1} \text{ cm}^{-1}$), the MLCT band of **Ru(bmptpphz)** is only visible as a shoulder at 470 nm ($\epsilon = 23 \times 10^3 \text{ M}^{-1} \text{ cm}^{-1}$). This shoulder is assigned to excitations into the four bright states, S_{13} , S_{14} , S_{15} , and S_{16} . The S_{13} and S_{16} , of MLCT character, lead to a population of both ligand spheres (**bmptpphz** and tbbpy), the excited state S_{14} refers to a MLCT excitation into the tbbpy ligand, while the S_{15} is associated with an ILCT from the *p*-anisyl-substituents to the phenazine moiety. Obviously, the novel **bmptpphz** ligand strongly contributes to the absorption in the visible region with a maximum at 416 nm ($\epsilon = 50 \times 10^3 \text{ M}^{-1} \text{ cm}^{-1}$). TDDFT calculations unravel the nature of this absorption band to be mainly correlated to the S_2 state; an ILCT transition with small contributions of a MLCT character. The main ILCT transition refers to an excitation from the π system of the 4-methoxyphenyl moieties (HOMO) to the π^* system of the phenazine (LUMO); detailed information



Scheme 2 Synthetic route for the introduction of the metal centres: (i) [(tbbpy)₂RuCl₂], ethanol–water, reflux, 18 h (78%); (ii) (acn)₂PdCl₂, dichloromethane, r. t., 4 d (61%).

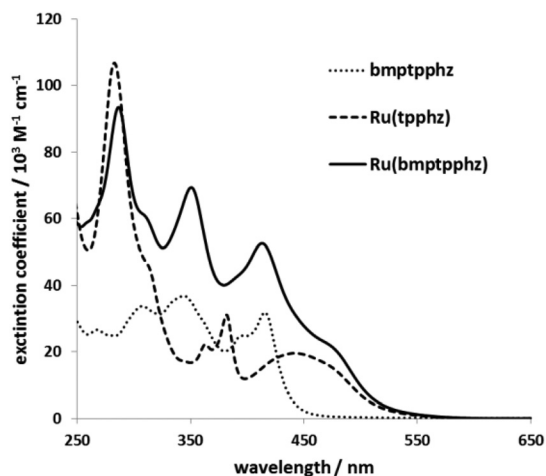


Fig. 3 UV-vis absorption spectra of **bmptpphz** (dotted), **Ru(tpphz)** (dashed) and **Ru(bmptpphz)** (solid) in acetonitrile.

Table 1 Absorption maxima, molar extinction coefficients, emission maxima and lifetimes of the ligand **bmptpphz** and the complex **Ru(bmptpphz)** in comparison to **tpphz** and **Ru(tpphz)PdCl₂**. All measurements were carried out in acetonitrile under aerated conditions

	Absorption $\lambda_{\text{max}}/\text{nm}$ ($\epsilon/10^3 \text{ M}^{-1} \text{ cm}^{-1}$)	Emission ^b $\lambda_{\text{max}}/\text{nm}$	Life time τ^c/ns
bmptpphz	265 (27), 305 (34), 341 (37), 395 (25), 413 (32)	500	—
Ru(bmptpphz)	287 (104), 312 (61), 351 (69), 414 (50), 470 (23)	632	152
Ru(tpphz)^a	285 (105), 314 (45), 381 (31), 445 (20)	638	150
Ru(bmptpphz)PdCl	286 (87), 330 (60), 447 (39)	664	—
Ru(tpphz)PdCl₂^a	283 (105), 379 (33), 444 (20)	—	—

^a Absorption and life time data were taken from Rau *et al.*^{29,30}

^b $\lambda_{\text{ex}}/\text{bmptpphz} = 340 \text{ nm}$ and 420 nm , $\lambda_{\text{ex}}/\text{Ru(bmptpphz)} = 470 \text{ nm}$, $\lambda_{\text{ex}}/\text{Ru(tpphz)} = 445 \text{ nm}$. ^c $\lambda_{\text{ex}}/\text{Ru(bmptpphz)} = 470 \text{ nm}$, $\lambda_{\text{ex}}/\text{Ru(tpphz)} = 445 \text{ nm}$.

concerning the TDDFT results are given in the ESI (Table S6 and Fig. S10[†]). The inversion of the MLCT and the ILCT states in calculations is mainly caused by the different CT nature of these states, while the assignment to the experimental

spectrum is based on the calculated oscillator strengths, resonance Raman simulations, as well as the absorption properties of the free **bmptpphz** ligand.

Emission spectra of the novel ligand **bmptpphz** were recorded in acetonitrile and were found to be independent of the excitation wavelength (see Table 1). Excitation at 320, as well as, 420 nm results in an emission maximum at 500 nm. The ruthenium complex **Ru(bmptpphz)** emits at 632 nm, which is almost identical to the unsubstituted **Ru(tpphz)** (638 nm) (see Table 1 and ESI Fig. S2[†]).

In addition, an excitation spectrum of **Ru(bmptpphz)** in acetonitrile was recorded to explore, whether the additional absorption at 416 nm, related to the arylated **tpphz** ligand, contributes to the population of the luminescent ³MLCT state (ESI Fig. S3[†]). Apparently, this is the case as the obtained excitation spectrum shows a maximum at 416 nm in the visible range identical to the absorption spectrum. Taking this experimental evidence and the results of the theoretical calculations into account an interesting conclusion can be drawn: obviously the excitation at 416 nm not only leads to the conventional MLCT states transferring electron density to the phen moiety,⁴³ but also the ILCT state significantly contributes to the population of the emissive MLCT state.

The emission lifetime of the excited state of **Ru(bmptpphz)** in acetonitrile of 152 ns is nearly identical to that of **Ru(tpphz)** (150 ns) under aerated conditions.³⁰

Furthermore, we have investigated the impact of the addition of the second metal centre on the photophysics. Regarding the absorption features of **Ru(bmptpphz)PdCl** in comparison with the mononuclear **Ru(bmptpphz)**, the absorption maximum in the visible range is shifted to a higher wavelength (447 nm) (see Table 1 and ESI Fig. S2[†]). This absorption wavelength is almost identical to that of the unsubstituted dinuclear **Ru(tpphz)PdCl₂**, which has a maximum at 444 nm attributed to the population of the ¹MLCT state.³¹ However, the extinction of **Ru(bmptpphz)PdCl** at 447 nm ($\epsilon = 39 \times 10^3 \text{ M}^{-1} \text{ cm}^{-1}$) is almost twice as high as the extinction of **Ru(tpphz)PdCl₂** at 444 nm ($\epsilon = 20 \times 10^3 \text{ M}^{-1} \text{ cm}^{-1}$), indicating that the enhanced absorption of visible light due to the novel substitution pattern of the bridging ligand is also maintained for the dinuclear complex. As mentioned above, the main absorption band in the visible range is shifted from 414 nm (**Ru(bmptpphz)**) to 447 nm (**Ru(bmptpphz)PdCl**) (see ESI

Table 2 Electrochemical data: half-wave potentials E (in V) (vs. Fc/Fc^+) in acetonitrile. The electrochemical measurements were carried out in anhydrous and argon purged solvent with a complex concentration of 1.0 mM and tetrabutylammonium hexafluorophosphate (0.1 mM) as supporting electrolyte

Substance	E_{ox}	E_{red}^I	E_{red}^{II}	E_{red}^{III}	E_{red}^{IV}	E_{red}^V	E_{red}^{VI}
Ru(bmptpphz)	0.82	-1.44	-1.90	-2.10	-2.27	-2.44	-2.90
Ru(tpphz)	0.80	-1.41	-1.92	-2.12	-2.23	-2.48	-2.90

Fig. S2†). A possible explanation for this bathochromic shift might be the induced in-plane alignment of one anisyl-substituent with respect to the tpphz-plane upon complexation and the consequential enhanced electron delocalisation.

In comparison to the mononuclear **Ru(bmptpphz)** a significant quenching of the emission intensity and a redshift of the emission maximum to 664 nm was observed for **Ru(bmptpphz)PdCl** (see ESI Fig. S2†). As typically found for hetero bimetallic ruthenium tpphz complexes, the second metal centre induces a $MLCT_{phen} \rightarrow MLCT_{pz}$ relaxation, which leads to a dominant population of a low-energy “dark state” located on the phenazine part, and so causes the decrease of the emission intensity and the bathochromic shift of the emission maximum.^{31,44,45}

Electrochemical properties

Cyclic voltammetry was used to obtain the redox potentials of **Ru(bmptpphz)** and **Ru(tpphz)** in acetonitrile (Table 2). Analogously to **Ru(tpphz)**, **Ru(bmptpphz)** shows the metal based oxidation wave at 0.82 V and multiple waves assignable to ligand based reductions, which are attributed to the reduction of the phenazine part (-1.44 V) and the ruthenium bound phen part of **tpphz** (-2.27 V), as well as to the first and second reduction of the terminal tbbpy ligands (-1.90, -2.10, and -2.44, -2.90 V).^{29,40} Apparently, the 4-methoxyphenyl-substituents have no significant effect on the redox potentials of **Ru(bmptpphz)** compared to **Ru(tpphz)**.

Raman spectroscopy

In order to monitor changes in the electron density distribution upon photoexcitation at the Franck–Condon point, resonance Raman (RR) spectroscopy is the method of choice.⁴⁶ In RR spectra normal modes, which are affected by the structural reorganization upon photoexcitation, are selectively enhanced. Hence, RR spectroscopy is an ideal tool to study the nature of the excited states in the Franck–Condon region.

RR spectra have been recorded using excitation wavelengths of 496, 488, 476, and 458 nm, *i.e.* in partial resonance with the MLCT band (at 470 nm) as well as the ILCT band (at 416 nm). Of particular interest is the investigation of the novel ILCT band in **Ru(bmptpphz)** and, hence, the RR spectrum recorded at 458 nm. This RR spectrum measured at 458 nm is depicted in Fig. 4 and compared to the calculated one; the RR spectra recorded at lower excitation energies as well as the non-resonant spectrum are illustrated in the ESI† along

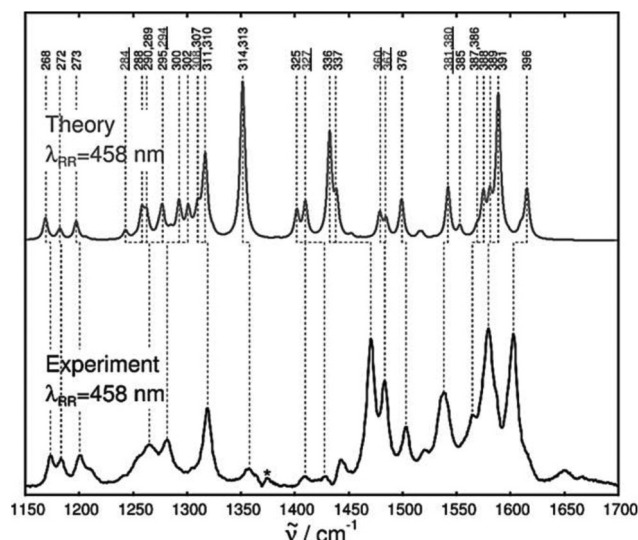


Fig. 4 Experimental and theoretical RR spectra for **Ru(bmptpphz)** in resonance with the states S_2 , S_{13} , S_{14} , S_{15} , S_{16} , S_{19} and S_{20} at the wavelength 458 nm. The experimental solvent band is indicated by an asterisk. The modes associated with vibrations located on the bipyridine ligands are given in underlined numbers, whereas the remaining numbers belong to modes associated with vibrations located on the tpphz ligand. A Lorentzian function with a FWHM of 5 cm^{-1} is employed to broaden the calculated transitions.

with detailed information concerning the computation of RR intensities.

The experimental and theoretical RR intensity patterns are in good agreement, while a mean absolute deviation from the calculated modes with respect to the Raman bands of 12 cm^{-1} was obtained. As can be seen by means of the simulated spectrum almost all intense Raman active modes are localized on the **bmptpphz** ligand, while only eight modes of small and medium intensity are centred on the tbbpy sphere. Analogous to **Ru(tpphz)** only the Raman features at 1483 cm^{-1} and 1538 cm^{-1} are assigned to intense modes centred on the tbbpy ligands. This result is consistent with the TDDFT results, showing that merely two of the seven bright excited states in this region are correlated to a charge transfer onto the tbbpy ligands, while all other bright states excite onto the **bmptpphz** ligand. Hence, a relaxation upon photoexcitation is mainly centred on the bridging ligand. The quantum chemical calculations show that the new absorption feature at 416 nm, correlated to the S_2 ILCT state, mainly contributes to the RR intensity pattern at 458 nm with its intense **bmptpphz** centred modes 313, 314, 336 and 391 (see ESI Table S7†).

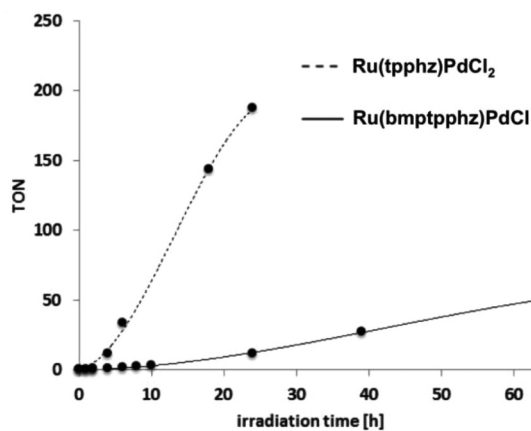


Fig. 5 Turnover numbers (TONs) of Ru(bmptpphz)PdCl (solid line) and Ru(tpphz)PdCl₂ (dashed line) in a mixture of acetonitrile, triethylamine and water under LED irradiation (470 nm).

Photocatalytic hydrogen production and mercury poisoning

To investigate the photocatalytic properties of Ru(bmptpphz)PdCl with regard to light-driven hydrogen production, the complex was dissolved in a catalytic mixture of the following composition: $c(\text{photocatalyst}) = 70 \mu\text{M}$, $V(\text{triethylamine}) = 0.6 \text{ ml}$ (2.2 M), $V(\text{acetonitrile}) = 1.2 \text{ mL}$ and $V(\text{water}) = 0.2 \text{ mL}$. Afterwards the solution was irradiated with LED light (470 nm, $35 \pm 5 \text{ mW cm}^{-2}$) and the amount of produced hydrogen was determined by headspace gas chromatography. In order to evaluate the effect of the novel substitution pattern of Ru(bmptpphz)PdCl, also the non-substituted Ru(tpphz)PdCl₂ was investigated under identical conditions for comparison.

Fig. 5 shows the catalytic activities of Ru(bmptpphz)PdCl and Ru(tpphz)PdCl₂ in terms of turnover numbers (TONs). For Ru(tpphz)PdCl₂ a significant induction period of roughly 2 hours was observed until a pronounced formation of hydrogen could be measured, which indicates the formation of a catalytically active species prior to catalytic turnover (see ESI Fig. S5†).^{32,33} It is apparent that Ru(bmptpphz)PdCl is less active giving a maximum TON of 50 after 64 hours of irradiation, compared to Ru(tpphz)PdCl₂, which shows a maximum TON of 187 after 24 hours.

From our point of view there are three possible reasons for the reduced activity of Ru(bmptpphz)PdCl: (1) as described above, the visible-light-driven ILCT implies an electron transfer from the anisyl-moiety onto the phenazine moiety of the bmptpphz ligand. Thus, electron density located in the periphery of the catalytic centre is withdrawn, which might lead to a less effective proton reduction. (2) Another explanation is the influence of the tridentate coordination of the Pd centre. As known from phen(Ph)₂PdCl (Ph = phenyl), which contains a similar tridentate coordination motif compared to Ru(bmptpphz)PdCl, the Pd core predominantly coordinates to the NC sphere with a C–Pd bond lengths of 1.985 Å, whereas the N–Pd distance (2.251 Å) of the opposing nitrogen is significantly larger, indicating the higher stability of the C–Pd bond.⁴⁷ In general, the photochemical reduction of the Pd(II)

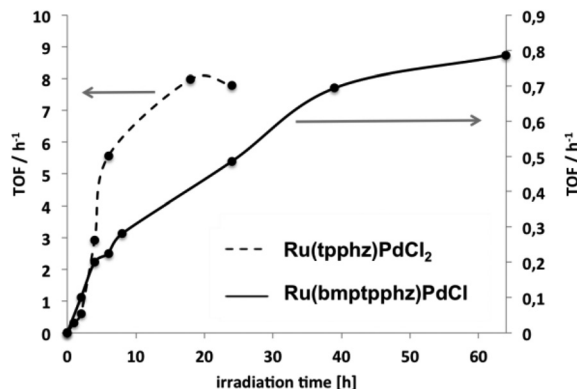


Fig. 6 Turnover frequencies (TOFs) of Ru(bmptpphz)PdCl (solid line) and Ru(tpphz)PdCl₂ (dashed line) in a mixture of acetonitrile, triethylamine and water under LED irradiation (470 nm).

centre to Pd(0) is a prerequisite for both, metal colloid formation and catalytic turnover of protons to hydrogen.³⁰ The cyclometallation in Ru(bmptpphz)PdCl will influence both, the redox properties of the Pd centre and the stability and reactivity of the metal centre in all oxidation states since Pd(0) forms stable bonds to organometallic ligands.⁴⁸ (3) Moreover, also the steric shielding by the anisyl-substituents might have an impact on the catalytic performance of the Pd centre. As reported in the literature, the catalytic activity of Pd as catalytic centre in a phen coordination sphere is significantly affected by the steric influence of substituents in 2,9-position (equivalent to the 2,17-position in bmptpphz).^{34,49}

The effect of the novel substitution pattern is also expressed by the turnover frequencies (TOF = TON/ t) of Ru(bmptpphz)PdCl illustrated in Fig. 6. For both, Ru(bmptpphz)PdCl and Ru(tpphz)PdCl₂, the TOF is constantly increasing with continuous irradiation, which might correlate to the progressive formation of Pd(0) colloids as already reported by Hammarström and co-workers.³² In case of Ru(tpphz)PdCl₂ the maximum TOF (7.9 h⁻¹) is reached already after 18 h of irradiation, whereas the TOF of Ru(bmptpphz)PdCl is still increasing with irradiation times over 40 h.

To evaluate the contribution of Pd(0) colloids to the formation of hydrogen, the mercury test was applied, known for its ability to deactivate metal colloids and particles by forming amalgams.⁵⁰ However, the mercury test must be treated with caution. As recently observed for a structurally related Ru–Pd photocatalysts, elemental Hg can decompose the photocatalyst already under non-catalytic conditions in pure acetonitrile.^{51,52} Thus, prior to investigations under catalytic conditions, the effect of Hg on the photocatalysts was tested under non-reductive conditions. Therefore both catalysts were dissolved in pure acetonitrile, a drop of liquid Hg was added and the suspension was allowed to stir for 7 h under exclusion of light. ¹H-NMR studies revealed that the unsubstituted Ru(tpphz)PdCl₂ reacts to the mononuclear Ru(tpphz) under the presence of Hg, meaning an extraction of the Pd(II) centre by Hg.³³ Interestingly, no reaction occurred with Ru(bmptpphz)PdCl under identical conditions underlining the increased stability of the

Pd centre (see ESI Fig. S7†). As a next step, a drop of liquid mercury was added to a catalytic mixture containing **Ru(bmptpphz)PdCl** as photocatalyst prior to irradiation. The result was a complete loss of catalytic activity (see ESI Table S4†). Independent from the irradiation time no hydrogen was produced in the presence of mercury. This is a first hint that photodecomposition and *in situ* generation of colloidal Pd might be an important part of the catalytic mechanism with **Ru(bmptpphz)PdCl**, however further methods of analysis have to be applied to confirm this assumption.^{52,53}

Conclusions

Herein, we reported on a novel structural modification of a tpphz based ligand. In this context, the first example of a regioselective asymmetric disubstitution in the 2,17-position of tpphz selectively influencing one coordination sphere of the potential bridging ligand was shown. Beside synthesis and characterisation of the novel ligand **bmptpphz**, also its complexation forming the mononuclear ruthenium complex **Ru(bmptpphz)** was successfully performed. Finally, the dinuclear **Ru(bmptpphz)PdCl** complex was synthesized and cyclometallation at the Pd centre had occurred. The photophysical and electrochemical investigations on the mononuclear complex **Ru(bmptpphz)** revealed analogies to the well-known **Ru(tpphz)** system. Interestingly **Ru(bmptpphz)** exhibits an enhanced absorption of visible light, which is also addressed by TDDFT simulations to the novel substitution pattern. Subsequently the dinuclear complex was tested towards its performance as hydrogen evolving photocatalyst. We could show that the novel substitution pattern has a significant influence on the catalytic performance of the Pd centre. Based on the results obtained from mercury poisoning experiments, the dissociation of palladium under photoexcitation and formation of palladium colloids as part of the catalysis mechanism must be taken into consideration.

Compared to **Ru(tpphz)PdCl₂**, **Ru(bmptpphz)PdCl** possesses an increased stability of the Pd(II) coordination sphere, caused by the tridentate coordination pocket and/or the steric shielding by the anisyl-rings.^{34,49} As the 2,9-arylated-phen sphere of **Ru(bmptpphz)** should be capable of stabilizing a large variety of metal cations like Ni²⁺, Co²⁺, Cu⁺ and Zn²⁺,⁵⁴ which are known to be active centres for catalytic hydrogen formation, a quite large number of potentially stable heterodinuclear photocatalysts is accessible.^{55–57}

Moreover, as the *p*-anisyl-substituents can easily be converted to hydroxyphenyl substituents, they provide the opportunity for further synthetic coupling, which makes **Ru(bmptpphz)** an interesting candidate concerning its application as building block for artificial molecular machines.⁵⁸ For instance, an interlock of **Ru(bmptpphz)** with catenane or rotaxane like architectures, which are used for the construction of molecular machines and motors, seems to be feasible.⁵⁹ Instead of a chemically induced exchange of metal ions, **Ru(bmptpphz)** could function as module for light-driven

reduction or oxidation of implemented metal centres to induce movement. In that concern, **Ru(bmptpphz)** might open a new pathway for the design of molecular machines fuelled by visible light.

Experimental

Instrumentation

NMR-spectra were measured with a Jeol EX-270 DELTA, a Jeol Lambda-400 and a Bruker DRX 400 spectrometer. The NMR spectra were recorded at 298 K and the NMR chemical shifts were referenced to the solvent peaks. MS analysis was performed on a Finnigan MAT SSQ 710, MAZ95XL or MAT 95 XP and on a Shimadzu LC-MS 2020 equipped with an electrospray ionisation source and a SPD-20A UV-vis detector. The UV-vis-spectra were recorded with a Varian CARY 50 Conc and a JASCO Spectrometer V-670. Quartz cells with a 10 mm path length were used. The emission spectra were recorded with a JASCO Spectrofluorometer FP-8500. Quartz cells with a 10 mm path length were used. The hydrogen evolved was measured by headspace GC on a Bruker Scion GC/MS, with a thermal conductivity detector (column: Mol. Sieve 5A 75 m × 0.53 mm I.D., oven temp. 70 °C, flow rate 22.5 ml min⁻¹, detector temp. 200 °C) with argon as carrier gas. The GC was calibrated by mixing different volumes of pure hydrogen together with argon into a Schlenk vessel. The obtained signal was plotted against the calibration curve and multiplied accordingly to obtain the total produced hydrogen content in the headspace. Resonance Raman (RR) spectra were excited by the visible lines of an Ar ion laser (Coherent, Innova 300C) and recorded with an Acton SpectraPro 2758i spectrometer (entrance slit width 100 μm, focal length 750 mm, grating 600 mm⁻¹). A 90 degree geometry was employed for the resonance Raman experiments. The Raman signals were detected using a liquid-nitrogen cooled CCD detector (SPEC-10, Roper Scientific). The band of acetonitrile at 1373 cm⁻¹ was used as a reference for normalizing intensities and wavenumbers. The recorded resonance Raman spectra were background corrected and the solvent spectrum was subtracted.

Photocatalysis

Photohydrogen production experiments were carried out using a custom-made air-cooling apparatus for maintaining room temperature (22 °C) under constant irradiation of the sample (ESI Fig. S4†). The solvents used were degassed with argon. The samples for the LED light irradiation experiments were prepared in GC vials (diameter = 45 × 14.75 mm) with a known headspace of 3 mL and a headspace-solution ratio of 3/2. Furthermore the GC vials were charged in the dark and under argon stream. After addition of acetonitrile containing the catalyst (*V* = 1.2 mL), triethylamine (*V* = 0.6 mL) and 10 vol% of water (*V* = 0.20 mL) the final catalyst concentration in acetonitrile was 70 μM. Subsequently, the GC vials were irradiated with blue LED light (470 nm, *P* = 35 ± 5 mW cm⁻²). After

irradiation, 200 μL samples were drawn from the headspace and injected immediately into the GC apparatus.

Stability of Ru(bmptpphz)PdCl towards liquid mercury

To test the stability of Ru(bmptpphz)PdCl towards elemental Hg under non-catalytic conditions, 2 mg (1.6 μmol) of the dinuclear complex were dissolved in 1.5 ml degassed deuterated acetonitrile under exclusion of oxygen and 300 μL liquid Hg were added. The suspension was stirred for 7 hours and afterwards the supernatant solution was transferred to a NMR tube.

Mercury test

The experimental setup for the catalyst poisoning with elemental mercury was analogous to the above described conditions for photocatalysis. In addition, a drop of elemental mercury (100 μl) was added to the catalytic mixture (see ESI Fig. S6†). Moreover, all samples (also those without mercury) were stirred constantly. Each sample was irradiated (sideward) for 24 hours and 99 hours. After irradiation, 200 μL samples were drawn from the headspace and injected immediately into the GC apparatus.

Quantum chemistry

The structural and electronic data of Ru(bmptpphz) were obtained from quantum chemistry calculations performed with the GAUSSIAN 09 program.⁶⁰ The geometry, vibrational frequencies, and normal coordinates of the ground state were calculated by means of DFT with the XC functional B3LYP.⁶¹ The 28-electron relativistic effective core potential MWB⁶² was used with its basis set for the ruthenium atom, that is, 4s, 4p, 4d and 5s electrons are treated explicitly, whereas the three first inner shells are described by the core pseudopotential. The 6-31G(d) double- ζ basis set⁶³ was employed for the ligands. To correct for the lack of anharmonicity and the approximate treatment of electron correlation, the harmonic frequencies were scaled by the factor 0.97.⁶⁴ The vertical excitation energies, oscillator strengths and analytical Cartesian energy derivatives of the excited states were obtained from TDDFT calculations within the adiabatic approximation with the same XC functional, pseudopotential and basis set. It was shown by several groups that B3LYP provides a balanced description of the absorption features of such complexes.^{43,65} The absorption spectra were simulated by determining the excitation energies and oscillator strengths of the 100 lowest singlet excited states. The effects of the interaction with a solvent (acetonitrile, $\epsilon = 35.688$, $n = 1.344$) on the geometry, frequencies, excitation energies and excited state gradients were taken into account by the integral equation formalism of the polarizable continuum model.⁶⁶ The nonequilibrium procedure of solvation was used for the calculation of the excitation energies and of the excited state gradients. Such procedure is well adapted for processes where only the fast reorganization of the electronic distribution of the solvent is important.

The resonance Raman (RR) spectra were calculated within the independent mode displaced harmonic oscillator model (IMDHOM), which assumes the electronic ground and excited states potentials to be harmonic oscillators with differing equilibrium positions, sharing the same set of vibrational modes. Within this approach the RR intensity for a fundamental transition $0 \rightarrow 1_l$ can be calculated from the Raman polarizability tensor.^{46,67–69}

$$(\alpha_{\alpha\beta})_{g0 \rightarrow g1_l} = \frac{1}{\hbar} \sum_e (\mu_{ge})_\alpha (\mu_{ge})_\beta \frac{\Delta_{e,l}}{\sqrt{2}} \{ \Phi_e(\omega_L) - \Phi_e(\omega_L - \omega_l) \} \quad (1)$$

where $(\mu_{ge})_\alpha$ is a component of the electronic transition dipole moment at the ground state equilibrium geometry, $\Delta_{e,l}$ is the dimensionless displacement of the eth excited state potential minimum with respect to the ground state for the l th normal coordinate and ω_L is the frequency of the incident light. The function $\Phi_e(\omega_L)$ is approximated by

$$\Phi_e(\omega_L) = \frac{1}{\omega_{g,e} - \omega_L - i\Gamma} \quad (2)$$

whereas $\omega_{g,e}$ is the vertical excitation energy from the electronic ground state g to the excited state e and Γ is a damping factor describing a homogeneous broadening. A value of Γ equal to 1750 cm^{-1} was assumed in the simulations to reproduce the experimental broadening. An excitation wavelength of 558 nm was employed to calculate the RR spectra, for which the vertical excitation energies $\omega_{g,e}$ were corrected so that experimental and theoretical absorption maxima coincide.

The absorption spectrum $A(\omega_L)$ is given by:

$$A(\omega_L) \propto \omega_L \sum_e (\mu_{ge})^2 \text{Im} \Phi_e(\omega_L) \quad (3)$$

The dimensionless displacement $\Delta_{e,l}$ of the excited state e is defined in the IMDHOM by the partial derivative of the excited state potential energy E^e along the normal mode Q_l evaluated at the ground state equilibrium geometry

$$\Delta_{e,l} = - \frac{1}{\sqrt{\hbar} \omega_l^{\frac{1}{2}}} \left(\frac{\partial E^e}{\partial Q_l} \right)_0 \quad (4)$$

These derivatives were obtained from the analytical derivatives of the excited state electronic energy (E^e) along the Cartesian coordinates.

More details about the calculation procedure of RR intensities can be found in ref. 46, 70 and references therein. The RR intensity has been calculated for an excitation wavelength of 458 nm and taking into account contributions from the singlet excited states S_2 , S_{13} , S_{14} , S_{15} , S_{16} , S_{19} , and S_{20} , while the excitation energies were corrected by +2000 cm^{-1} (S_2) and -3500 cm^{-1} (S_{13} , S_{14} , S_{15} , and S_{16}), respectively.

Synthesis and characterisation

The complete synthesis procedure, including the synthesis of bmpphenO₂ is shown in the ESI.†

bmptpphz. To a boiling solution of bmpphenO_2 (0.46 g, 1.08 mmol) in methanol (250 ml) $\text{phen}(\text{NH}_2)_2$ (0.31 g, 1.49 mmol) was added in portions over 2 hours. The mixture was refluxed for 8 hours, whereby the bright yellow product precipitated. The product was separated by filtration and washed with water, methanol and acetone and dried *in vacuo*. Yield = 76% (0.49 g); $M(\text{C}_{38}\text{H}_{24}\text{N}_6\text{O}_2) = 596.6 \text{ g mol}^{-1}$; MS (DEI in acetonitrile + trifluoroacetic acid): $m/z = 596 [\text{M} - \text{H}]^-$; $^1\text{H-NMR}$ (270 MHz, CDCl_3 + trifluoroacetic acid, 295 K): $\delta = 10.21$ (d, 2 H, $J = 7.96 \text{ Hz}$, c), 10.10 (d, 2 H, $J = 8.87 \text{ Hz}$, c'), 9.36 (d, 2 H, $J = 4.87 \text{ Hz}$, a), 8.64 (d, 2 H, $J = 8.86 \text{ Hz}$, b'), 8.36 (dd, 2 H, $J = 5.20$ and $J = 8.33 \text{ Hz}$, b), 8.25 (d, 4 H, $J = 8.69 \text{ Hz}$, o), 7.27 (d, 4 H, $J = 8.71 \text{ Hz}$, m), 4.01 (s, 6 H, OMe) ppm;

Ru(bmptpphz). The ligand **bmptpphz** (0.49 g, 0.82 mmol) was suspended in ethanol–water (100 ml/100 ml) and heated to reflux. Afterwards $[(\text{tbbpy})_2\text{RuCl}_2]$ (0.60 g, 0.85 mmol) in ethanol–water (50 ml/50 ml) was added during 1 hour. The orange-brown suspension was refluxed for 18 hours more and subsequently filtered while hot to remove unreacted ligand. Afterwards the solution was concentrated under reduced pressure using a rotary evaporator and the crude product was precipitated by adding 100 ml of an aqueous solution of NH_4PF_6 (0.80 g, 5.0 mmol). The precipitated brown-reddish solid was separated by filtration and washed with water, diethyl ether and dried *in vacuo*.

Finally, the ruthenium complex was purified by column chromatography on silica (dichloromethane–methanol 1:1 v/v). The product elutes as first band.

Yield = 78% (1.0 g); $M(\text{C}_{74}\text{H}_{72}\text{F}_{12}\text{N}_{10}\text{O}_2\text{P}_2\text{Ru}) = 1524.4 \text{ g mol}^{-1}$; MS (FD in acetonitrile): $m/z = 1380 [\text{M} - \text{PF}_6]^+$; $^1\text{H-NMR}$ (400 MHz, CD_3CN , 295 K, $c = 0.01 \text{ M}$): $\delta = 9.42$ (d, 2 H, $J = 8.18 \text{ Hz}$, c), 9.19 (d, 2 H, $J = 8.82 \text{ Hz}$, c'), 8.63 (d, 2 H, $J = 1.86 \text{ Hz}$, 3'), 8.60 (d, 2 H, $J = 1.81 \text{ Hz}$, 3), 8.13 (dd, 2 H, $J = 4.96, 1.25 \text{ Hz}$, a), 8.07 (d, 4 H, $J = 8.57 \text{ Hz}$, o), 8.01 (d, 2 H, $J = 8.54 \text{ Hz}$, b'), 7.92 – 7.64 (m, 6H, 6', b, 6), 7.55 (dd, 2 H, $J = 5.90, 2.14 \text{ Hz}$, 5'), 7.41 (d, 2 H, $J = 6.14 \text{ Hz}$, 5), 6.68 (d, 4 H, $J = 8.43 \text{ Hz}$, m), 3.73 (s, 6 H, MeO), 1.51 (s, 18 H, *tert* butyl), 1.37 (s, 18 H, *tert* butyl) ppm; $^{13}\text{C-NMR}$ (100 MHz, CD_3CN , 295 K): $\delta = 29.58, 29.68, 35.53, 35.58, 55.08, 118.84, 118.87, 121.76, 121.82, 123.93, 124.9, 126.45, 128.27, 129.67, 130.37, 133.03, 133.44, 146.73, 149.25, 151.20, 151.29, 152.75, 156.98, 157.12, 157.26, 161.13, 163.09$ ppm.

Ru(bmptpphz)PdCl. 20 mg (0.013 mmol) **Ru(bmptpphz)** were dissolved in 15 ml dichloromethane and 3.9 mg (0.015 mmol) $\text{Pd}(\text{acn})_2\text{Cl}_2$ were added. The reaction mixture was stirred for 4 days at room temperature. After 1 day another 1.95 mg (7.5 μmol) $\text{Pd}(\text{acn})_2\text{Cl}_2$ were added. Subsequently, the solvent was evaporated at room temperature and the residue was dissolved acetonitrile and applied to a column with silica as solid phase and washed with water. Afterwards the dinuclear complex was eluted with acetonitrile–water + KNO_3 (saturated) 15:1 v/v. The fractions were combined and the solution was concentrated under reduced pressure at room temperature. Following this, an aqueous solution of NH_4PF_6 (0.08 mmol) was added to precipitate the product, which was

finally separated by filtration and washed with water, diethyl ether and dried *in vacuo*.

Yield = 61% (0.013 g); $M(\text{C}_{74}\text{ClH}_{71}\text{F}_{12}\text{N}_{10}\text{O}_2\text{P}_2\text{PdRu}) = 1665.3 \text{ g mol}^{-1}$; MS (ESI in acetonitrile): $m/z = 965.9 [2\text{M} - 3\text{PF}_6]^{3+}$, $687.4 [\text{M} - 2\text{PF}_6]^{2+}$, $617.4 [\text{M} - 2\text{PF}_6 - \text{PdCl}]^{2+}$; $^1\text{H-NMR}$ (400 MHz, CD_3CN , 295 K, $c = 8.5 \text{ mM}$): $\delta = 9.91$ (d, 1H, $J = 8.2 \text{ Hz}$, c''), 9.85 (d, 1H, $J = 8.4 \text{ Hz}$, c'''), 9.79 (d, $J = 8.3 \text{ Hz}$, c), 9.65 (d, 1H, $J = 8.7 \text{ Hz}$, c'), 8.60 (s, 2H, 3/3'''), 8.55 (s, 2H, 3'/3''), 8.32 (dd, 1H, $J = 5.3, 1.2 \text{ Hz}$, a'), 8.27 (dd, 1H, $J = 5.3, 1.2 \text{ Hz}$, a), 8.24 (d, 1H, $J = 8.4 \text{ Hz}$, b'''), 8.08 (dd, 1H, $J = 8.2, 5.4 \text{ Hz}$, b''), 8.02 (dd, 1H, $J = 8.2, 5.3 \text{ Hz}$, b), 7.88 (d, 1H, $J = 8.9 \text{ Hz}$, b'), 7.85 – 7.73 (m, 4H, 6/6''/o), 7.70 (d, 1H, $J = 6.2 \text{ Hz}$, 6''), 7.66 (d, 1H, $J = 6.1 \text{ Hz}$, 6'), 7.58 – 7.50 (m, 2H, 5/5'''), 7.48 – 7.27 (m, 3H, 5'/5''/*), 7.24 (d, 2H, $J = 8.6 \text{ Hz}$, m), 6.19 (s, 1H, *), 5.99 (s, 1H, *), 3.96 (s, 3H, OMe), 3.44 (s, 3H, OMe'), 1.48 (s, 9H, *tert* butyl), 1.47 (s, 9H, *tert* butyl), 1.35 (s, 18H, *tert* butyl).

Acknowledgements

This research is supported by German Research Association (DFG SFB 583, GRK 1626) and the COST Action CM1202, PERSPECT-H2O. J. G. is grateful to the 7th Framework Programme of the European Union. All the calculations have been performed at the Universitätsrechenzentrum of the Friedrich-Schiller University of Jena and at the HP computers of the Theoretical Chemistry group.

Notes and references

- N. S. Lewis and D. G. Nocera, *Proc. Natl. Acad. Sci. U. S. A.*, 2003, **103**, 15729.
- P. Ritterskamp, A. Kuklya, M. A. Wustkamp, K. Kerpen, C. Weidenthaler and M. Demuth, *Angew. Chem., Int. Ed.*, 2007, **46**, 7770.
- Z. Zhang, J. Long, L. Yang, W. Chen, W. Dai, X. Fu and X. Wang, *Chem. Sci.*, 2011, **2**, 1826.
- F. Gärtner, B. Sundararaju, A.-E. Surkus, A. Boddien, B. Loges, H. Junge, P. H. Dixneuf and M. Beller, *Angew. Chem., Int. Ed.*, 2009, **48**, 9962.
- S. Oishi, *J. Mol. Catal.*, 1978, **39**, 225.
- R. Bauer and H. A. F. Werner, *Int. J. Hydrogen Energy*, 1994, **19**, 497.
- J. Hawecker, J.-M. Lehn and R. Ziessel, *Nouv. J. Chim.*, 1983, **7**, 271.
- Y. Na, M. Wang, J. Pan, P. Zhang, B. Åkermark and L. Sun, *Inorg. Chem.*, 2008, **47**, 2805.
- H. Ozawa and K. Sakai, *Chem. Commun.*, 2011, **47**, 2227.
- E. Amouyal, *Sol. Energy Mater. Sol. Cells*, 1995, **38**, 249.
- A. Guskov, J. Kern, A. Gabdulkhakov, M. Broser, A. Zouni and W. Saenger, *Nat. Struct. Mol. Biol.*, 2009, **16**, 334.
- L. Duan, Y. Xu, P. Zhang, M. Wang and L. Sun, *Inorg. Chem.*, 2010, **49**, 209.
- J. T. Muckerman, D. E. Polyansky, T. Wada, K. Tanaka and E. Fujita, *Inorg. Chem.*, 2008, **47**, 1787.

- 14 F. Liu, J. J. Concepcion, J. W. Jurss, T. Cardolaccia, J. L. Templeton and T. J. Meyer, *Inorg. Chem.*, 2008, **47**, 1727.
- 15 S. W. Gersten, G. J. Samuels and T. J. Meyer, *J. Am. Chem. Soc.*, 1982, **104**, 4029.
- 16 C. Sens, I. Romero, M. Rodríguez, A. Llobet, T. Parella and J. Benet-Buchholz, *J. Am. Chem. Soc.*, 2004, **126**, 7798.
- 17 J.-M. Lehn, M. Kirch and J.-P. Sauvage, *Helv. Chim. Acta*, 1979, **62**, 1345.
- 18 V. Balzani, *Photochem. Photobiol. Sci.*, 2003, **2**, 459.
- 19 S. Rau, D. Walther and J. G. Vos, *Dalton Trans.*, 2007, 915.
- 20 C. Li, M. Wang, J. Pan, P. Zhang, R. Zhang and L. Sun, *J. Organomet. Chem.*, 2009, **694**, 2814.
- 21 H. Ozawa, M. Haga and K. Sakai, *J. Am. Chem. Soc.*, 2006, **128**, 4926.
- 22 A. Fihri, V. Artero, A. Pereira and M. Fontecave, *Dalton Trans.*, 2008, 5567.
- 23 A. Fihri, V. Artero, M. Razavet, C. Baffert, W. Leibl and M. Fontecave, *Angew. Chem., Int. Ed.*, 2008, **47**, 564.
- 24 M. Elvington, J. Brown, S. M. Arachchige and K. J. Brewer, *J. Am. Chem. Soc.*, 2007, **129**, 10644.
- 25 M. Karnahl, C. Kuhnt, F. W. Heinemann, M. Schmitt, S. Rau, J. Popp and B. Dietzek, *Chem. Phys.*, 2012, **393**, 65.
- 26 M. Karnahl, C. Kuhnt, F. Ma, A. Yartsev, M. Schmitt, B. Dietzek, S. Rau and J. Popp, *ChemPhysChem*, 2011, 2101.
- 27 R. Konduri, H. Ye, F. M. MacDonnell, S. Serroni, S. Campagna and K. Rajeshwar, *Angew. Chem., Int. Ed.*, 2002, **41**, 3185.
- 28 L. Zedler, J. Guthmuller, I. Rabelo de Moraes, S. Kupfer, S. Kriek, M. Schmitt, J. Popp, S. Rau and B. Dietzek, *Chem. Commun.*, 2014, **50**, 5227.
- 29 M. Karnahl, S. Tschierlei, C. Kuhnt, B. Dietzek, M. Schmitt, J. Popp, M. Schwalbe, S. Kriek, H. Görls, F. W. Heinemann and S. Rau, *Dalton Trans.*, 2010, **39**, 2359.
- 30 S. Rau, B. Schäfer, D. Gleich, E. Anders, M. Rudolph, M. Friedrich, H. Görls, W. Henry and J. G. Vos, *Angew. Chem., Int. Ed.*, 2006, **45**, 6215.
- 31 S. Tschierlei, M. Presselt, C. Kuhnt, A. Yartsev, T. Pascher, V. Sundström, M. Karnahl, M. Schwalbe, B. Schäfer, S. Rau, M. Schmitt, B. Dietzek and J. Popp, *Chem. – Eur. J.*, 2009, **15**, 7678.
- 32 P. Lei, M. Hedlund, R. Lomoth, H. Rensmo, O. Johansson and L. Hammarström, *J. Am. Chem. Soc.*, 2007, **130**, 26.
- 33 M. Pfeffer, B. Schäfer, C. Kuhnt, M. Schmitt, J. Popp, J. Guthmuller, G. Smolentsev, J. Uhlig, E. Nazarenko, V. Sundström, L. González, B. Dietzek and S. Rau, manuscript in preparation.
- 34 D. Takeuchi, A. Yasuda and K. Osakada, *Dalton Trans.*, 2003, 2029.
- 35 J. Frey, T. Kraus, V. Heitz and J.-P. Sauvage, *Chemistry*, 2007, **13**, 7584.
- 36 E. C. Constable, R. P. G. Henney, T. A. Leese and D. A. Tocher, *J. Chem. Soc., Dalton Trans.*, 1990, 443.
- 37 S. W. Lai, T. C. Cheung, M. C. Chan, K. K. Cheung, S. M. Peng and C. M. Che, *Inorg. Chem.*, 2000, **39**, 255.
- 38 F. Neve, M. Ghedini and A. Crispini, *Chem. Commun.*, 1996, 2463.
- 39 F. Neve, A. Crispini, C. Di Pedro and S. Campagna, *Organometallics*, 2002, **21**, 3511.
- 40 J. Bolger, A. Gourdon, E. Ishow and J.-P. Launay, *Inorg. Chem.*, 1996, **35**, 2937.
- 41 S. Bodige, A. S. Torres, D. J. Maloney, D. Tate, G. Kinsel, A. Walker and F. M. MacDonnell, *J. Am. Chem. Soc.*, 1997, **119**, 10364.
- 42 C. Kuhnt, M. Karnahl, M. Schmitt, S. Rau, B. Dietzek and J. Popp, *Chem. Commun.*, 2011, **47**, 3820.
- 43 S. Tschierlei, M. Karnahl, M. Presselt, B. Dietzek, J. Guthmuller, L. González, M. Schmitt, S. Rau and J. Popp, *Angew. Chem., Int. Ed.*, 2010, **49**, 3981.
- 44 L. Flamigni, S. Encinas, F. Barigelletti, F. M. MacDonnell, K.-J. Kim, F. Puntoriero and S. Campagna, *Chem. Commun.*, 2000, 1185.
- 45 C. Chiorboli, M. a J. Rodgers and F. J. Scandola, *J. Am. Chem. Soc.*, 2003, **125**, 483.
- 46 M. Wächtler, J. Guthmuller, L. González and B. Dietzek, *Coord. Chem. Rev.*, 2012, **256**, 1479.
- 47 M. Kuritani, S. Tashiro and M. Shionoya, *Chem. – Asian J.*, 2013, **8**, 1368.
- 48 M. Schwalbe, H. Schreer, J. Langer, H. Görls and D. Walther, *J. Organomet. Chem.*, 2006, **691**, 4868.
- 49 G.-J. ten Brink, I. W. C. E. Arends, M. Hoogenraad, G. Verspui and R. A. Sheldon, *Adv. Synth. Catal.*, 2003, **345**, 1341.
- 50 D. R. Anton and R. H. Crabtree, *Organometallics*, 1983, **2**, 855.
- 51 G. Singh Bindra, M. Schulz, A. Paul, S. Soman, R. Groarke, J. Inglis, M. T. Pryce, W. R. Browne, S. Rau, B. J. Maclean and J. G. Vos, *Dalton Trans.*, 2011, **40**, 10812.
- 52 V. Artero and M. Fontecave, *Chem. Soc. Rev.*, 2013, **42**, 2338.
- 53 J. A. Widegren and R. G. Finke, *J. Mol. Catal. A: Chem.*, 2003, **198**, 317.
- 54 A.-M. Albrecht-Gary, C. Dietrich-Buchecker, Z. Saad and J.-P. Sauvage, *J. Am. Chem. Soc.*, 1988, **40**, 1467.
- 55 M. P. McLaughlin, T. M. McCormick, R. Eisenberg and P. L. Holland, *Chem. Commun.*, 2011, **47**, 7989.
- 56 J. Halpern, *J. Phys. Chem.*, 1959, **63**, 398.
- 57 W. Sattler and G. J. Parkin, *Am. Chem. Soc.*, 2012, **134**, 17462.
- 58 V. Balzani, A. Credi, F. Raymo and J. Stoddart, *Angew. Chem., Int. Ed.*, 2000, **39**, 3348.
- 59 C. Dietrich-Buchecker, M. C. Jimenez-Molero, V. Sartor and J.-P. Sauvage, *Pure Appl. Chem.*, 2003, **75**, 1383.
- 60 M. J. Frisch, G. W. Trucks, H. B. Schlegel, G. E. Scuseria, M. A. Robb, J. R. Cheeseman, G. Scalmani, V. Barone, B. Mennucci, G. A. Petersson, H. Nakatsuji, M. Caricato, X. Li, H. P. Hratchian, A. F. Izmaylov, J. Bloino, G. Zheng, J. L. Sonnenberg, M. Hada, M. Ehara, K. Toyota, R. Fukuda, J. Hasegawa, M. Ishida, T. Nakajima, Y. Honda, O. Kitao, H. Nakai, T. Vreven, J. A. Montgomery Jr., J. E. Peralta, F. Ogliaro, M. Bearpark, J. J. Heyd, E. Brothers, K. N. Kudin, V. N. Staroverov, R. Kobayashi, J. Normand,

- K. Raghavachari, A. Rendell, J. C. Burant, S. S. Iyengar, J. Tomasi, M. Cossi, N. Rega, J. M. Millam, M. Klene, J. E. Knox, J. B. Cross, V. Bakken, C. Adamo, J. Jaramillo, R. Gomperts, R. E. Stratmann, O. Yazyev, A. J. Austin, R. Cammi, C. Pomelli, J. W. Ochterski, R. L. Martin, K. Morokuma, V. G. Zakrzewski, G. A. Voth, P. Salvador, J. J. Dannenberg, S. Dapprich, A. D. Daniels, Ö. Farkas, J. B. Foresman, J. V. Ortiz, J. Cioslowski and D. J. Fox, *Gaussian 09, Revision D.01*, Gaussian, Inc., Wallingford, CT, 2009.
- 61 (a) A. D. Becke, *J. Chem. Phys.*, 1993, **98**, 5648; (b) C. Lee, W. Yang and R. G. Parr, *Phys. Rev. B: Condens. Matter*, 1988, **37**, 785.
- 62 D. Andrae, U. Häußermann, M. Dolg, H. Stoll and H. Preuß, *Theor. Chim. Acta*, 1990, **77**, 123.
- 63 P. C. Hariharan and J. A. Pople, *Theor. Chim. Acta*, 1973, **28**, 213–222.
- 64 J. P. Merrick, D. Moran and L. Radom, *J. Phys. Chem.*, 2007, **111**, 11683.
- 65 J. Guthmuller and L. González, *Phys. Chem. Chem. Phys.*, 2010, **12**, 14812.
- 66 J. Tomasi, B. Mennucci and R. Cammi, *Chem. Rev.*, 2005, **105**, 2999.
- 67 J. B. Page and D. L. Tonks, *J. Chem. Phys.*, 1981, **75**, 5694.
- 68 W. L. Peticolas and T. Rush, *J. Comput. Chem.*, 1995, **16**, 1261.
- 69 J. Guthmuller and L. González, *Phys. Chem. Chem. Phys.*, 2010, **12**, 14812.
- 70 S. Kupfer, M. Wächtler, J. Guthmuller, J. Popp, B. Dietzek and L. González, *J. Phys. Chem. C*, 2012, **116**, 19968.